ESI for

Chiral Spin-crossover complexes based on an enantiopure Schiff base ligand with three chiral carbon centers

Alejandro Regueiro,[a] Víctor García-López,[a] Alicia Forment-Aliaga[a] and Miguel Clemente-León *[a]

Fig. S1 Experimental (red line) and simulated (blue line) powder X-ray diffraction patterns of [Fe(*RR*-*S*-L_2)$(NCSe)_2$] (a), [Fe(*SS*-*R*-L_2)$(NCSe)_2$] (b), [Fe(*RR*-*S*-L_2)$(NCS)_2$] (c) and [Fe(*SS*-*R*-L_2)$(NCSe)_2$] (d).

Fig. S2 TGA of [Fe(*RR*-*S*-L_2)$(NCSe)_2$] (black line), [Fe(*SS*-*R*-L_2)$(NCSe)_2$] (red line), [Fe(*RR*-*S*-L_2)$(NCS)_2$] (blue line) and [Fe(*SS*-*R*-L_2)$(NCSe)_2$] (green line).

Table S1 Crystal data and structure refinement for [Fe(*RR*-*S*-L_2)$(NCSe)_2$].

Table S2 Crystal data and structure refinement for [Fe(*SS*-*R*-L_2)$(NCSe)_2$].

Table S3 Crystal data and structure refinement for refinement for [Fe(*RR*-*S*-L_2)$(NCS)_2$].

Table S4 Crystal data and structure refinement for refinement for [Fe(*SS*-*R*-L_2)$(NCS)_2$].

Fig. S3 Asymmetric unit of [Fe(*RR*-*S*-L_2)$(NCSe)_2$] (left) and [Fe(*SS*-*R*-L_2)$(NCSe)_2$] (right) at 120 K (top), 300 K (medium) and 400 K (bottom). Fe (brown), Se (orange), C (black), N (blue) and O (red). Hydrogen atoms have been omitted for clarity.

Fig. S4 Asymmetric unit of [Fe(*RR*-*S*-L_2)$(NCSe)_2$] (left) and [Fe(*SS*-*R*-L_2)$(NCSe)_2$] (right) at 90 K (top), 150 K (*RR*-*S*-) and 130 K (*SS*-*R*-) (medium) and 200 K (bottom). Fe (brown), S (yellow), C (black), N (blue) and O (red). Hydrogen atoms have been omitted for clarity.

Fig. S5 Thermal variation of the average Fe-N distances for [Fe(*RR*-*S*-L_2)$(NCS)_2$] (green circles) and [Fe(*SS*-*R*-L_2)$(NCS)_2$] (red circles) (**a**) and [Fe(*RR*-*S*-L_2)$(NCSe)_2$] (green circles) and [Fe(*SS*-*R*-L_2)$(NCSe)_2$] (red circles) (**b**). Thermal variation of unit cell volumes for [Fe(*RR*-*S*-L_2)$(NCS)_2$] (green circles) and [Fe(*SS*-*R*-L_2)$(NCS)_2$] (red circles) (**c**) and [Fe(*RR*-*S*-L_2)$(NCSe)_2$] (green circles) and [Fe(*SS*-*R*-L_2)$(NCSe)_2$] (red circles) (**d**).

Table S5 Bond lengths and distortion parameters of [Fe(*RR*-*S*- and *SS*-*R*-L_2)$(NCX)_2$] at variable temperatures. Dashed values correspond to the second configuration of the complexes found in some of the structures.

Fig. S6 Chains of complexes in the structure of [Fe(*RR*-*S*-L_2)$(NCSe)_2$] (top) and [Fe(*SS*-*R*-L_2)$(NCSe)_2$] (bottom) at 120 K linked through intermolecular interactions (red dashed lines).

Fig. S7 UV-vis spectra and High Tension (HT) Voltage of CD measurements for 1 mM $CHCl_3$ solutions of [Fe(*RR*-*S*-L_2)$(NCSe)_2$] and [Fe(*SS*-*R*-L_2)$(NCSe)_2$] (left) and [Fe(*RR*-*S*-L_2)$(NCS)_2$] and [Fe(*SS*-*R*-L_2)$(NCS)_2$] (right).

Fig. S8 Images of $CHCl_3$ and MeCN solutions of [Fe(*RR*-*S*- or *SS*-*R*-L_2)$(NCX)_2$].

Fig. S9 Absorbance spectra of [Fe(*RR*-*S*- or *SS*-*R*-L_2)$(NCX)_2$] in the solid state.

Fig. S10 Time variation of $\chi_M T$ for [Fe(*RR*-*S*-L_2)$(NCSe)_2$] (green circles) and [Fe(*SS*-*R*-L_2)$(NCSe)_2$] (red circles) (**top**), [Fe(*RR*-*S*-L_2)$(NCS)_2$] (green circles) and [Fe(*SS*-*R*-L_2)$(NCS)_2$] (red circles) (**bottom**) after irradiation at 10 K with 808 nm in the LIESST experiments from **Fig. 5**. [Fe(*RR*-*S*-L_2)$(NCSe)_2$] and [Fe(*SS*-*R*-L_2)$(NCS)_2$] were first irradiated with 660 nm (3.4 h for [Fe(*RR*-*S*-L_2)$(NCSe)_2$] and 0.5 h for [Fe(*SS*-*R*-L_2)$(NCS)_2$]).

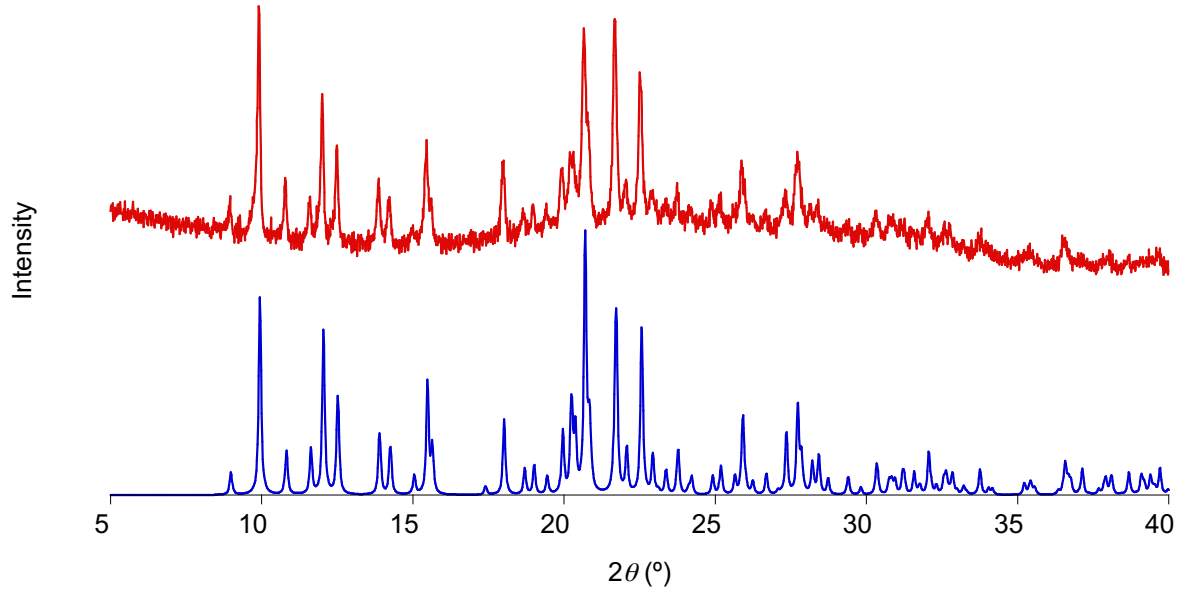
Intensity
5
10
15
20
25
30
35
40
2θ (°)

(a)

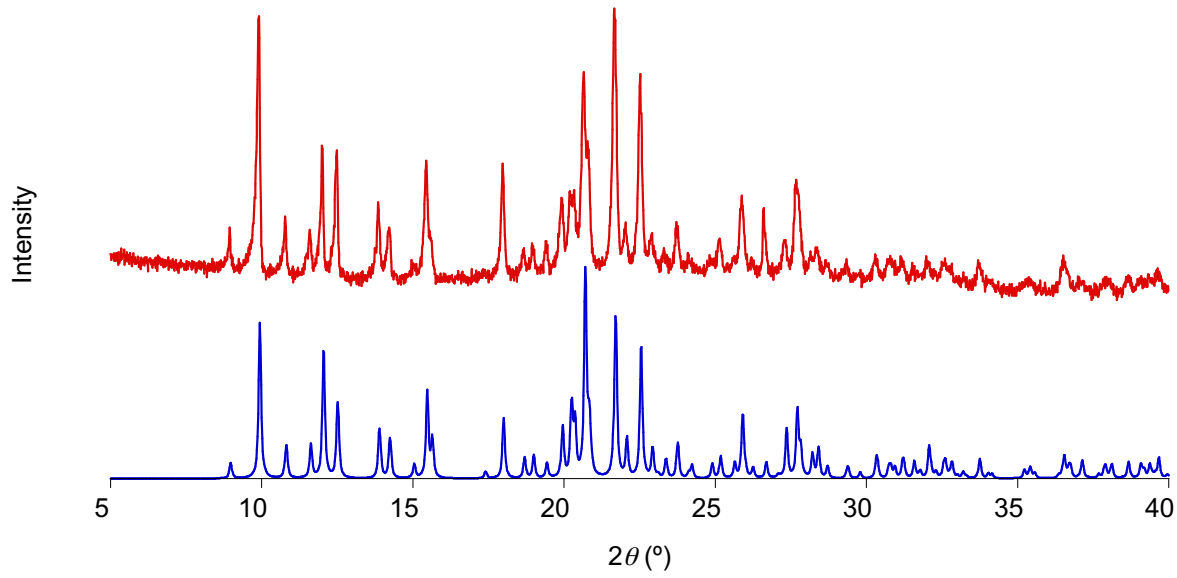
Intensity
5
10
15
20
25
30
35
40
2θ (°)

(b)

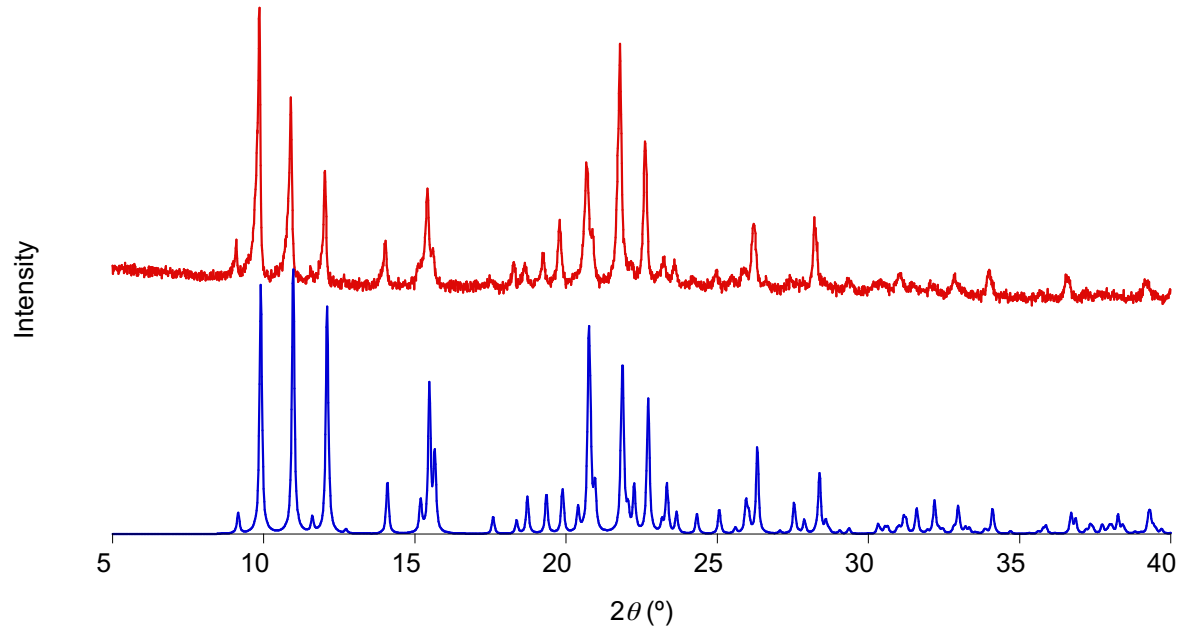

(c)

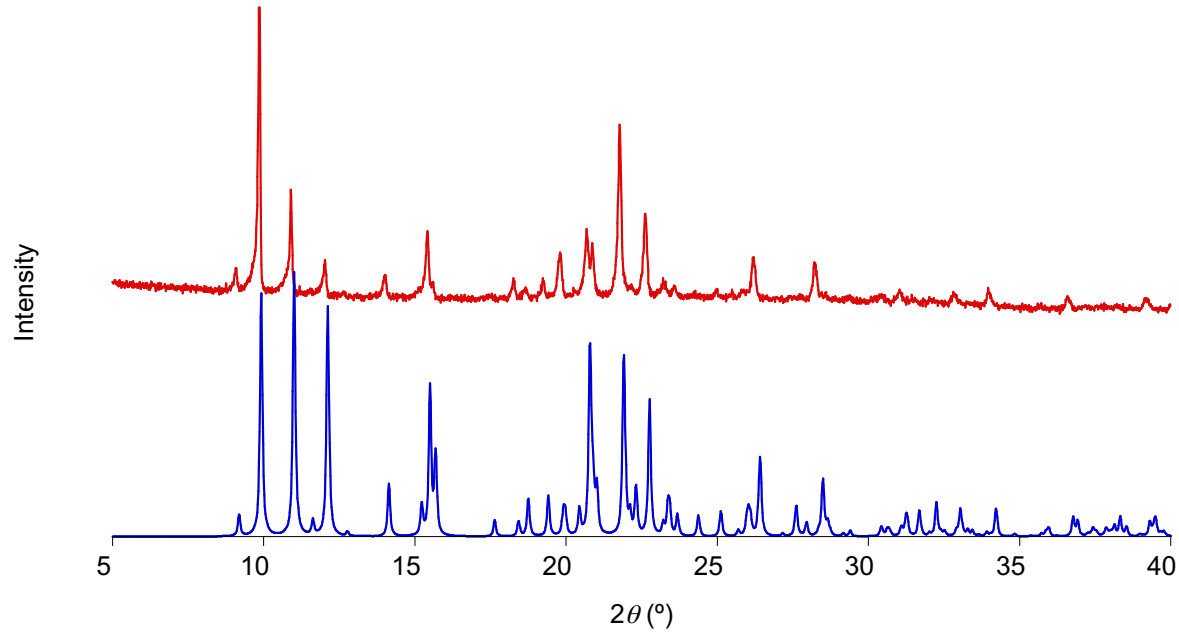

(d)

Fig. S1 Experimental (red line) and simulated (blue line) powder X-ray diffraction patterns of [Fe(*RR*-*S*-L_2)$(NCSe)_2$] (a), [Fe(*SS*-*R*-L_2)$(NCSe)_2$] (b), [Fe(*RR*-*S*-L_2)$(NCS)_2$] (c) and [Fe(*SS*-*R*-L_2)$(NCS)_2$] (d).

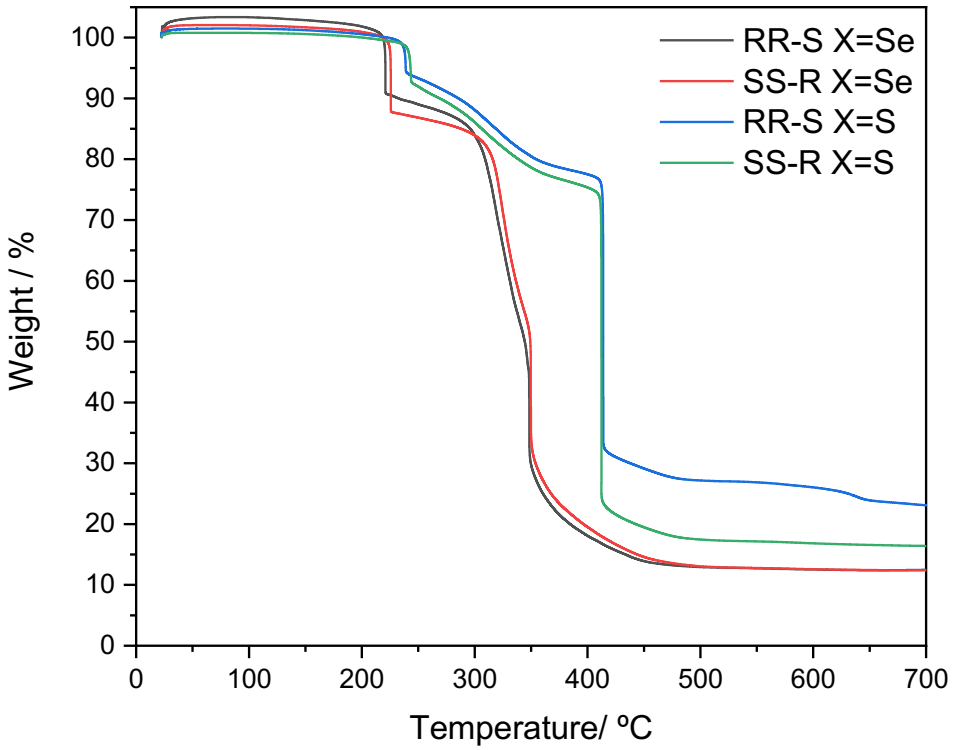

Fig. S2 TGA of [Fe(*RR*-*S*-L_2)$(NCSe)_2$] (black line), [Fe(*SS*-*R*-L_2)$(NCSe)_2$] (red line), [Fe(*RR*-*S*-L_2)$(NCS)_2$] (blue line) and [Fe(*SS*-*R*-L_2)$(NCS)_2$] (green line).

Table S1 Crystal data and structure refinement for [Fe(*RR*-*S*-L_2)$(NCSe)_2$].

Empirical formula	$C_{23}H_{26}FeN_6OSe_2$	$C_{23}H_{26}FeN_6OSe_2$	$C_{23}H_{26}FeN_6OSe_2$	$C_{23}H_{26}FeN_6OSe_2$	$C_{23}H_{26}FeN_6OSe_2$
Formula weight	616.27	616.27	616.27	616.27	616.27
Temperature/K	119.90(14)	159.90(14)	199.95(10)	299.95(10)	400.00(10)
Crystal system	monoclinic	monoclinic	monoclinic	monoclinic	monoclinic
Space group	$P2_1$	$P2_1$	$P2_1$	$P2_1$	$P2_1$
a/Å	8.7881(4)	8.8057(4)	8.8390(6)	8.9654(5)	9.0291(6)
b/Å	14.4060(5)	14.4435(5)	14.5072(8)	14.6855(7)	14.7931(10)
c/Å	9.8793(4)	9.8922(5)	9.9010(7)	9.9205(6)	9.9962(7)
α/°	90	90	90	90	90
β/°	98.194(4)	98.118(5)	98.031(6)	97.425(5)	97.426(7)
γ/°	90	90	90	90	90
Volume/Å^3	1237.96(9)	1245.53(10)	1257.15(14)	1295.19(12)	1323.98(16)
Z	2	2	2	2	2
ϱ_{calc}g/cm^3	1.653	1.643	1.628	1.580	1.546
μ/mm^{-1}	3.577	3.555	3.522	3.419	3.345
F(000)	616.0	616.0	616.0	616.0	616.0
Crystal size/mm^3	0.19 × 0.1 × 0.1	0.19 × 0.1 × 0.1	0.19 × 0.1 × 0.1	0.19 × 0.1 × 0.1	0.19 × 0.1 × 0.1
Radiation	MoKα (λ = 0.71073)	MoKα (λ = 0.71073)	MoKα (λ = 0.71073)	MoKα (λ = 0.71073)	MoKα (λ = 0.71073)
2Θ range for data collection/°	5.656 to 60.922	5.642 to 48.92	5.616 to 61.136	5.548 to 61.062	5.724 to 61.23
Index ranges	-12 ≤ h ≤ 11, -20 ≤ k ≤ 19, -13 ≤ l ≤ 13	-8 ≤ h ≤ 10, -15 ≤ k ≤ 14, -10 ≤ l ≤ 9	-12 ≤ h ≤ 12, -20 ≤ k ≤ 20, -14 ≤ l ≤ 13	-12 ≤ h ≤ 12, -20 ≤ k ≤ 20, -13 ≤ l ≤ 14	-12 ≤ h ≤ 12, -20 ≤ k ≤ 20, -14 ≤ l ≤ 14
Reflections collected	11745	5620	21103	21667	22116
Independent reflections	6663 [R_{int} = 0.0443, R_{sigma} = 0.0965]	2934 [R_{int} = 0.0480, R_{sigma} = 0.0891]	6964 [R_{int} = 0.0613, R_{sigma} = 0.0890]	7197 [R_{int} = 0.0709, R_{sigma} = 0.1114]	7367 [R_{int} = 0.1142, R_{sigma} = 0.1731]
Data/restraints/parameters	6663/1/299	2934/1/299	6964/1/299	7197/9/312	7367/1/299
Goodness-of-fit on F^2	0.994	1.023	1.001	0.966	0.943
Final R indexes [I>=2σ (I)]	R_1 = 0.0566, wR_2 = 0.0932	R_1 = 0.0494, wR_2 = 0.0776	R_1 = 0.0550, wR_2 = 0.0922	R_1 = 0.0595, wR_2 = 0.0982	R_1 = 0.0675, wR_2 = 0.1219
Final R indexes [all data]	R_1 = 0.0893, wR_2 = 0.1067	R_1 = 0.0725, wR_2 = 0.0880	R_1 = 0.1119, wR_2 = 0.1108	R_1 = 0.1777, wR_2 = 0.1339	R_1 = 0.2473, wR_2 = 0.1869
Largest diff. peak/hole / e Å^{-3}	0.99/-0.59	0.49/-0.36	0.64/-0.37	0.45/-0.36	0.36/-0.33
Flack parameter	0.005(9)	-0.007(16)	0.016(8)	0.016(9)	-0.020(18)

Table S2 Crystal data and structure refinement for [Fe(*SS*-*R*-L_2)$(NCSe)_2$].

Empirical formula	$C_{23}H_{26}FeN_6OSe_2$	$C_{23}H_{25}FeN_6OSe_2$	$C_{23}H_{26}FeN_6OSe_2$	$C_{23}H_{26}FeN_6OSe_2$
Formula weight	616.27	615.26	616.27	616.27
Temperature/K	120.00(10)	300.00(10)	340.00(14)	400.6(8)
Crystal system	monoclinic	monoclinic	monoclinic	monoclinic
Space group	$P2_1$	$P2_1$	$P2_1$	$P2_1$
a/Å	8.7851(6)	8.9670(5)	9.0034(12)	9.0416(18)
b/Å	14.3976(10)	14.6787(8)	14.735(3)	14.803(3)
c/Å	9.8896(6)	9.9286(5)	9.9527(14)	10.017(2)
α/°	90	90	90	90
β/°	98.260(7)	97.401(5)	97.345(13)	97.447(18)
γ/°	90	90	90	90
Volume/Å^3	1237.90(14)	1295.95(12)	1309.5(4)	1329.4(5)
Z	2	2	2	2
ϱ_{calc}g/cm^3	1.653	1.577	1.563	1.540
μ/mm^{-1}	3.577	3.417	3.381	3.331
F(000)	616.0	614.0	616.0	616.0
Crystal size/mm^3	0.23 × 0.04 × 0.02	0.23 × 0.04 × 0.02	0.23 × 0.04 × 0.02	0.23 × 0.04 × 0.02
Radiation	MoKα (λ = 0.71073)	MoKα (λ = 0.71073)	MoKα (λ = 0.71073)	MoKα (λ = 0.71073)
2Θ range for data collection/°	5.66 to 61.012	5.764 to 61.01	5.748 to 48.98	6.342 to 61.276
Index ranges	-12 ≤ h ≤ 11, -20 ≤ k ≤ 20, -12 ≤ l ≤ 13	-12 ≤ h ≤ 12, -20 ≤ k ≤ 20, -14 ≤ l ≤ 13	-9 ≤ h ≤ 10, -13 ≤ k ≤ 14, -10 ≤ l ≤ 11	-12 ≤ h ≤ 12, -19 ≤ k ≤ 21, -12 ≤ l ≤ 14
Reflections collected	11793	21626	5812	10855
Independent reflections	6661 [R_{int} = 0.0769, R_{sigma} = 0.1748]	7211 [R_{int} = 0.1224, R_{sigma} = 0.2146]	2778 [R_{int} = 0.1119, R_{sigma} = 0.2066]	6842 [R_{int} = 0.1739, R_{sigma} = 0.5612]
Data/restraints/parameters	6661/1/299	7211/9/267	2778/1/299	6842/1/259
Goodness-of-fit on F^2	0.988	0.943	0.934	0.866
Final R indexes [I>=2σ (I)]	R_1 = 0.0742, wR_2 = 0.0913	R_1 = 0.0725, wR_2 = 0.0870	R_1 = 0.0652, wR_2 = 0.0953	R_1 = 0.0898, wR_2 = 0.1608
Final R indexes [all data]	R_1 = 0.1580, wR_2 = 0.1194	R_1 = 0.2576, wR_2 = 0.1323	R_1 = 0.1890, wR_2 = 0.1447	R_1 = 0.4421, wR_2 = 0.3073
Largest diff. peak/hole / e Å^{-3}	0.88/-0.61	0.52/-0.37	0.30/-0.28	0.42/-0.35
Flack parameter	0.004(15)	-0.009(15)	-0.01(3)	0.00(4)

Table S3 Crystal data and structure refinement for refinement for [Fe(*RR*-*S*-L_2)$(NCS)_2$].

Empirical formula	$C_{23}H_{26}FeN_6OS_2$	$C_{23}H_{25}FeN_6OS_2$	$C_{23}H_{26}FeN_6OS_2$	$C_{23}H_{26}FeN_6OS_2$	$C_{23}H_{26}FeN_6OS_2$
Formula weight	522.47	521.46	522.47	522.47	522.47
Temperature/K	92.05(10)	149.8(4)	199.90(14)	249.90(14)	299.95(10)
Crystal system	monoclinic	monoclinic	monoclinic	monoclinic	monoclinic
Space group	$P2_1$	$P2_1$	$P2_1$	$P2_1$	$P2_1$
a/Å	8.8449(5)	8.9161(4)	8.9560(5)	8.9762(8)	8.9966(4)
b/Å	14.4593(7)	14.5306(6)	14.5794(8)	14.6245(11)	14.6464(6)
c/Å	9.6066(4)	9.6438(4)	9.6812(4)	9.7166(6)	9.7359(3)
α/°	90	90	90	90	90
β/°	96.395(4)	96.383(4)	96.444(5)	96.509(7)	96.448(3)
γ/°	90	90	90	90	90
Volume/Å^3	1220.95(10)	1241.67(9)	1256.12(11)	1267.30(17)	1274.76(9)
Z	2	2	2	2	2
ϱ_{calc}g/cm^3	1.421	1.395	1.381	1.369	1.361
μ/mm^{-1}	0.817	0.803	0.794	0.787	0.782
F(000)	544.0	542.0	544.0	544.0	544.0
Crystal size/mm^3	0.79 × 0.21 × 0.08	0.79 × 0.21 × 0.08	0.79 × 0.21 × 0.08	0.79 × 0.21 × 0.08	0.79 × 0.21 × 0.08
Radiation	MoKα (λ = 0.71073)	MoKα (λ = 0.71073)	MoKα (λ = 0.71073)	MoKα (λ = 0.71073)	MoKα (λ = 0.71073)
2Θ range for data collection/°	5.634 to 59.808	5.904 to 59.664	5.876 to 59.59	5.858 to 59.718	5.848 to 59.71
Index ranges	-12 ≤ h ≤ 11, -20 ≤ k ≤ 20, -13 ≤ l ≤ 12	-11 ≤ h ≤ 12, -20 ≤ k ≤ 20, -12 ≤ l ≤ 13	-12 ≤ h ≤ 11, -20 ≤ k ≤ 20, -13 ≤ l ≤ 13	-11 ≤ h ≤ 12, -20 ≤ k ≤ 20, -13 ≤ l ≤ 13	-12 ≤ h ≤ 11, -20 ≤ k ≤ 20, -13 ≤ l ≤ 13
Reflections collected	11925	12097	12244	12380	12358
Independent reflections	6170 [R_{int} = 0.0330, R_{sigma} = 0.0661]	6271 [R_{int} = 0.0344, R_{sigma} = 0.0690]	6340 [R_{int} = 0.0332, R_{sigma} = 0.0711]	6386 [R_{int} = 0.0372, R_{sigma} = 0.0798]	6456 [R_{int} = 0.0393, R_{sigma} = 0.0868]
Data/restraints/parameters	6170/5/352	6271/6/322	6340/1/362	6386/7/341	6456/7/362
Goodness-of-fit on F^2	1.023	1.034	1.023	1.005	1.012
Final R indexes [I>=2σ (I)]	R_1 = 0.0487, wR_2 = 0.0912	R_1 = 0.0538, wR_2 = 0.1025	R_1 = 0.0500, wR_2 = 0.0844	R_1 = 0.0538, wR_2 = 0.0887	R_1 = 0.0545, wR_2 = 0.0815
Final R indexes [all data]	R_1 = 0.0694, wR_2 = 0.1034	R_1 = 0.0839, wR_2 = 0.1206	R_1 = 0.0929, wR_2 = 0.1030	R_1 = 0.1109, wR_2 = 0.1133	R_1 = 0.1319, wR_2 = 0.1110
Largest diff. peak/hole / e Å^{-3}	0.47/-0.29	0.49/-0.33	0.43/-0.31	0.38/-0.28	0.30/-0.24
Flack parameter	0.002(11)	-0.002(13)	0.005(12)	0.020(13)	-0.016(14)

Table S4 Crystal data and structure refinement for refinement for [Fe(*SS-R*-L_2)$(NCS)_2$].

Empirical formula	$C_{23}H_{26}FeN_6OS_2$	$C_{23}FeN_6OS_2H_{0.5}$	$C_{23}H_{26}FeN_6OS_2$	$C_{23}H_{26}FeN_6OS_2$
Formula weight	522.47	496.76	522.47	522.47
Temperature/K	92(3)	132(4)	202(3)	401(1)
Crystal system	monoclinic	monoclinic	monoclinic	monoclinic
Space group	$P2_1$	$P2_1$	$P2_1$	$P2_1$
a/Å	8.8517(3)	8.9004(4)	8.9656(5)	9.0250(4)
b/Å	14.4554(5)	14.5127(8)	14.5928(9)	14.7281(8)
c/Å	9.5844(3)	9.6200(4)	9.6785(5)	9.7940(4)
α/°	90	90	90	90
β/°	96.324(3)	96.242(4)	96.291(5)	96.401(4)
γ/°	90	90	90	90
Volume/$Å^3$	1218.91(7)	1235.24(10)	1258.64(12)	1293.71(11)
Z	2	2	2	2
$\varrho_{calc}g/cm^3$	1.424	1.336	1.379	1.341
μ/mm^{-1}	0.818	0.805	0.792	0.771
F(000)	544.0	493.0	544.0	544.0
Crystal size/mm^3	0.23 × 0.06 × 0.04	0.23 × 0.06 × 0.04	0.23 × 0.06 × 0.04	0.23 × 0.06 × 0.04
Radiation	MoKα (λ = 0.71073)	MoKα (λ = 0.71073)	MoKα (λ = 0.71073)	MoKα (λ = 0.71073)
2Θ range for data collection/°	5.948 to 55.468	5.614 to 59.728	5.584 to 59.53	5.532 to 59.79
Index ranges	-10 ≤ h ≤ 10, -18 ≤ k ≤ 18, -10 ≤ l ≤ 12	-7 ≤ h ≤ 12, -20 ≤ k ≤ 19, -13 ≤ l ≤ 11	-12 ≤ h ≤ 7, -20 ≤ k ≤ 19, -11 ≤ l ≤ 13	-12 ≤ h ≤ 7, -20 ≤ k ≤ 20, -11 ≤ l ≤ 13
Reflections collected	8677	10926	11180	11534
Independent reflections	4813 [R_{int} = 0.0435, R_{sigma} = 0.0999]	6147 [R_{int} = 0.0441, R_{sigma} = 0.1034]	6261 [R_{int} = 0.0435, R_{sigma} = 0.1059]	6472 [R_{int} = 0.0618, R_{sigma} = 0.1371]
Data/restraints/parameters	4813/1/292	6147/9/312	6261/7/312	6472/1/299
Goodness-of-fit on F^2	1.021	1.005	1.004	0.995
Final R indexes [I>=2σ (I)]	R_1 = 0.0589, wR_2 = 0.0875	R_1 = 0.0634, wR_2 = 0.0954	R_1 = 0.0635, wR_2 = 0.0910	R_1 = 0.0617, wR_2 = 0.0864
Final R indexes [all data]	R_1 = 0.0936, wR_2 = 0.1030	R_1 = 0.1173, wR_2 = 0.1167	R_1 = 0.1322, wR_2 = 0.1167	R_1 = 0.2071, wR_2 = 0.1407
Largest diff. peak/hole / e $Å^{-3}$	0.48/-0.31	0.45/-0.30	0.48/-0.26	0.43/-0.26
Flack parameter	-0.001(16)	0.000(15)	0.022(15)	0.01(2)

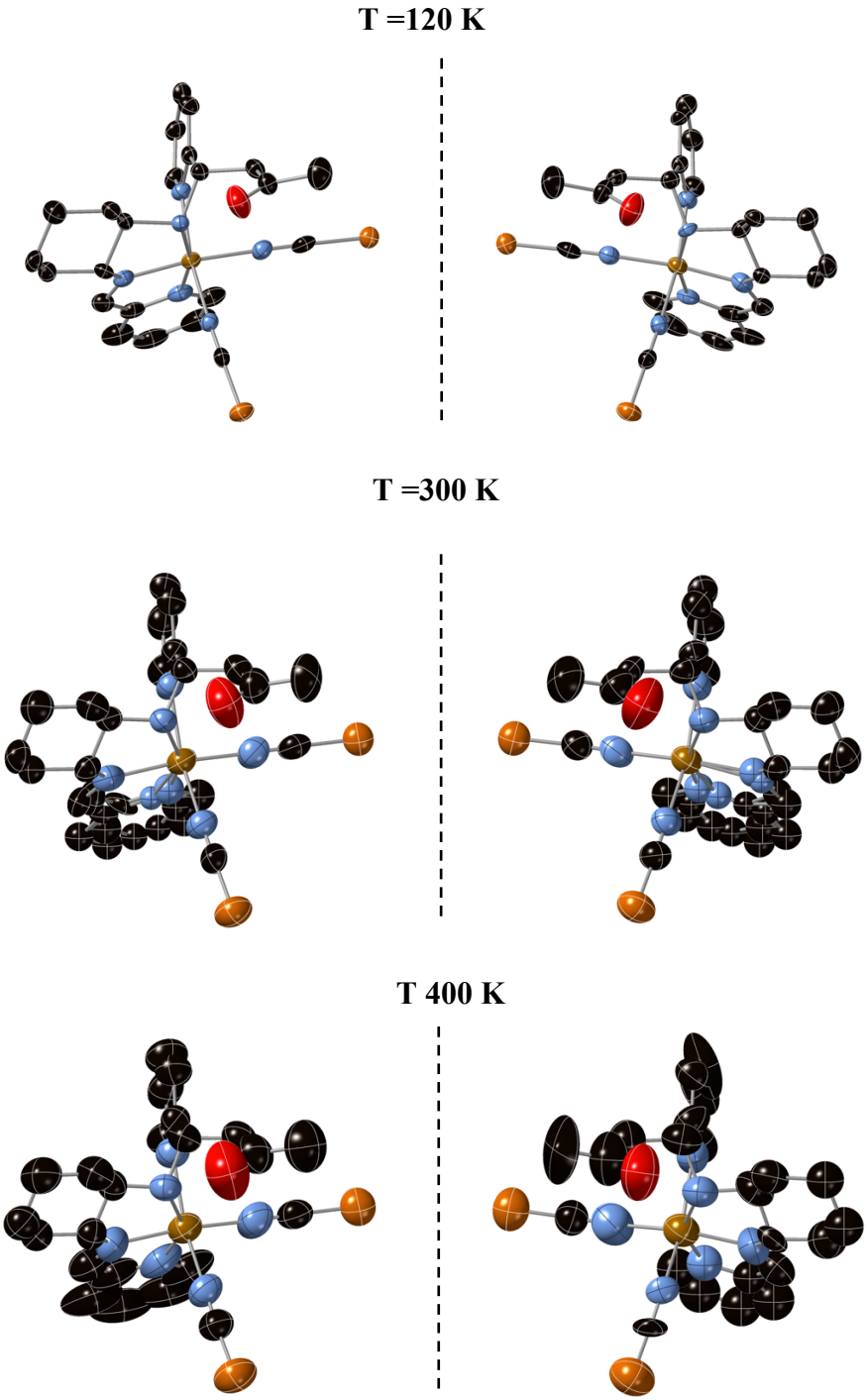

Fig. S3 Asymmetric unit of [Fe(*RR*-*S*-L$_2$)(NCSe)$_2$] (left) and [Fe(*SS*-*R*-L$_2$)(NCSe)$_2$] (right) at 120 K (top), 300 K (medium) and 400 K (bottom). Fe (brown), Se (orange), C (black), N (blue) and O (red). Hydrogen atoms have been omitted for clarity.

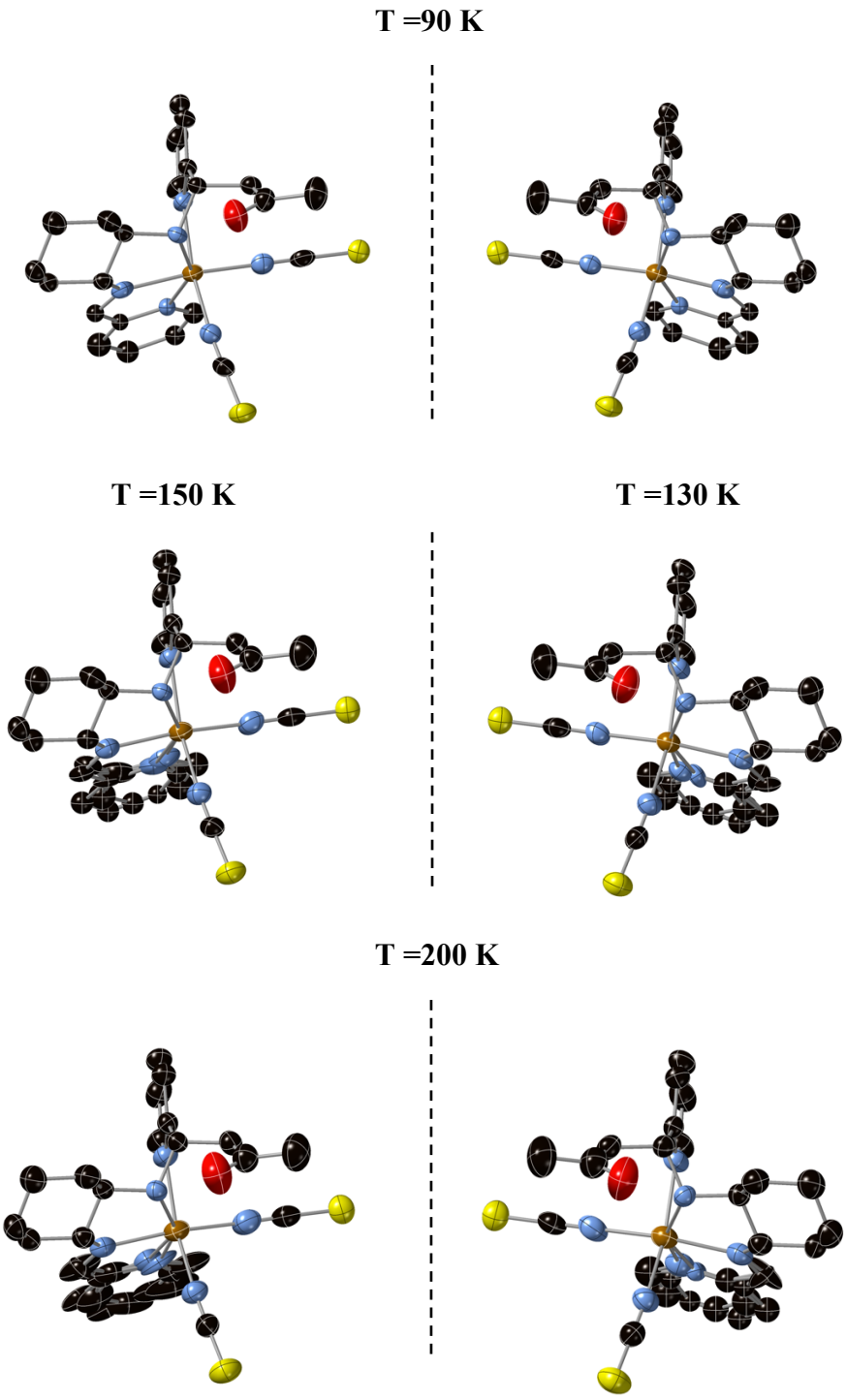

Fig. S4 Asymmetric unit of [Fe(*RR*-*S*-L_2)$(NCSe)_2$] (left) and [Fe(*SS*-*R*-L_2)$(NCSe)_2$] (right) at 90 K (top), 150 K (*RR*-*S*-) and 130 K (*SS*-*R*-) (medium) and 200 K (bottom). Fe (brown), S (yellow), C (black), N (blue) and O (red). Hydrogen atoms have been omitted for clarity.

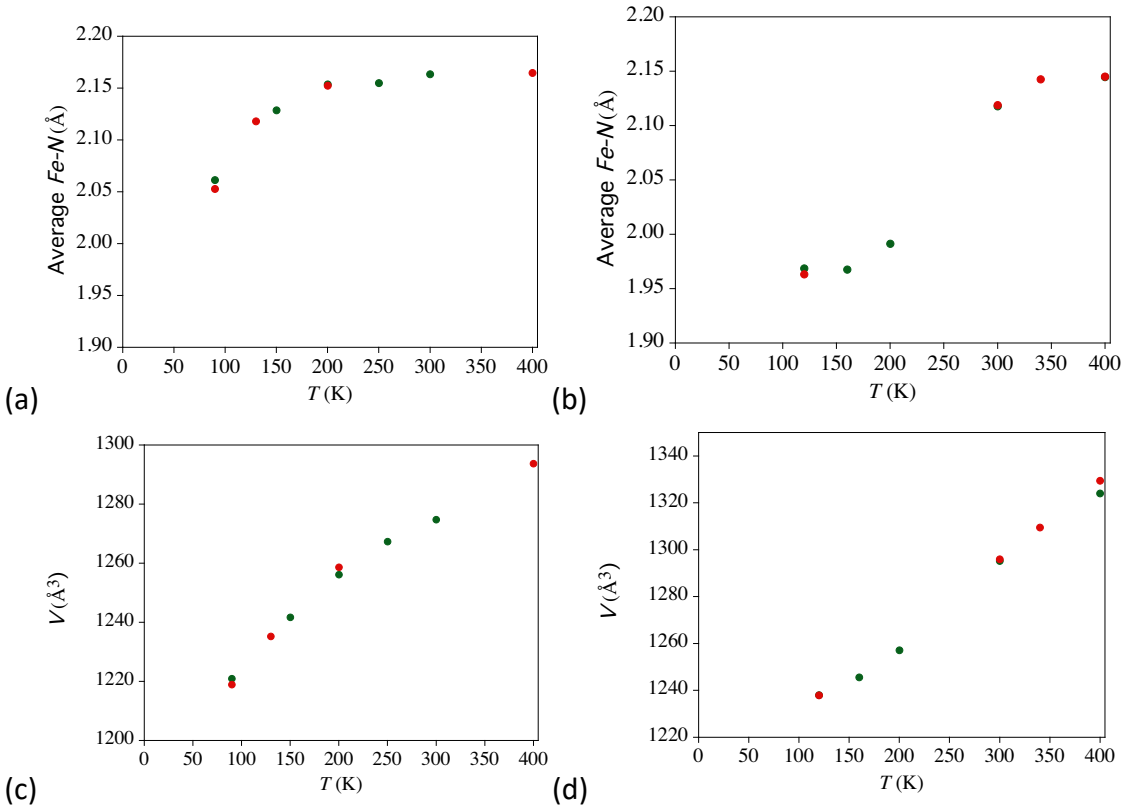

Fig. S5 Thermal variation of the average Fe-N distances for [Fe(*RR*-*S*-L_2)$(NCS)_2$] (green circles) and [Fe(*SS*-*R*-L_2)$(NCS)_2$] (red circles) (**a**) and [Fe(*RR*-*S*-L_2)$(NCSe)_2$] (green circles) and [Fe(*SS*-*R*-L_2)$(NCSe)_2$] (red circles) (**b**). Thermal variation of unit cell volumes for [Fe(*RR*-*S*-L_2)$(NCS)_2$] (green circles) and [Fe(*SS*-*R*-L_2)$(NCS)_2$] (red circles) (**c**) and [Fe(*RR*-*S*-L_2)$(NCSe)_2$] (green circles) and [Fe(*SS*-*R*-L_2)$(NCSe)_2$] (red circles) (**d**).

Table S5 Bond lengths and distortion parameters of [Fe(*RR*-*S*- and *SS*-*R*-L_2)$(NCX)_2$] at variable temperatures. Dashed values correspond to the second configuration of the complexes found in some of the structures.

	[Fe(*RR*-*S*-L_2)$(NCS)_2$]	90 K	150 K	200 K	250 K	300 K
Fe-N (Å)		2.098(3) 2.011(4) 2.149(4) 2.016(4) **2.10(4)** 2.014(5) 2.06(4)	2.173(4) 2.215(4) **2.280(10)** 2.086(5) 2.052(6) 2.012(11) 2.103(5)	2.204(4) 2.128(5) 2.242(4) **2.322(11)** 2.096(5) 2.067(6) 2.046(10)	2.219(4) 2.247(4) 2.133(6) **2.335(13)** 2.098(5) 2.071(7) 2.042(12)	2.253(5) 2.229(4) 2.138(6) **2.343(14)** 2.097(6) 2.063(7) 2.058(12)
Σ (°)		80.29 **101.09**	93.41 **110.99**	97.61 **115.91**	98.74 **116.64**	99.77 **117.72**
Θ (°)		228.91 **283.16**	267.61 **317.63**	280.88 **332.88**	285.73 **337.04**	285.82 **340.46**
	[Fe(*SS*-*R*-L_2)$(NCS)_2$]	90 K	130 K	200 K	400 K	
Fe-N (Å)		2.094(5) 2.003(6) 2.024(6) 2.141(5) 1.925(13) 2.005(7) **2.173(15)**	2.152(4) 2.060(6) 2.188(5) 2.063(6) **2.248(13)** 2.038(7) 1.979(12)	2.210(5) 2.238(5) 2.127(6) **2.305(13)** 2.096(6) 2.066(7) 2.030(13)	2.232(7) 2.191(10) 2.266(7) 2.142(9) 2.098(9) 2.059(11)	
Σ (°)		79.65 **97.40**	87.57 **105.21**	96.81 **114.42**	106.65	
Θ (°)		220.44 **275.55**	254.58 **307.31**	278.03 **330.06**	311.83	
	[Fe(*RR*-*S*-L_2)$(NCSe)_2$]	120 K	160 K	200 K	300 K	400 K
Fe-N (Å)		2.048(6) 1.993(6) 1.890(6) 1.963(7) 1.953(7) 1.964(7)	2.058(9) 1.993(10) 1.942(12) 1.880(10) 1.971(12) 1.961(13)	2.026(6) 2.082(6) 1.917(7) 1.976(7) 1.968(7) 1.978(8)	2.173(7) 2.214(7) 2.065(9) 1.946(19) 2.074(10) 2.052(11) **2.323(19)**	2.237(10) 2.086(12) 2.213(12) 2.167(17) 2.053(15) 2.112(14)
Σ (°)		71.28	69.90	76.07	90.83 **109.07**	102.98
Θ (°)		186.46	186.68	204.01	261.42 **313.09**	301.59
	[Fe(*SS*-*R*-L_2)$(NCSe)_2$]	120 K	300 K	340 K	400 K	
Fe-N (Å)		2.047(9) 1.982(8) 1.960(10) 1.884(10) 1.955(11) 1.951(9)	2.205(9) 2.169(9) 1.87(3) 1.97(3) 2.095(11) 2.047(15) **2.31(4)** **2.22(3)**	2.240(18) 2.17(2) 2.09(3) 2.16(3) 2.11(2) 2.08(3)	2.10(3) 2.21(3) 2.21(3) 2.20(3) 2.09(3) 2.05(4)	
Σ (°)		70.50	91.54 **110.93**	103.72	99.10	
Θ (°)		185.01	274.56 **304.14**	298.33	313.97	

$\Theta = \sum|\theta i - 60|$; $\Sigma = \sum|\phi i - 90|$

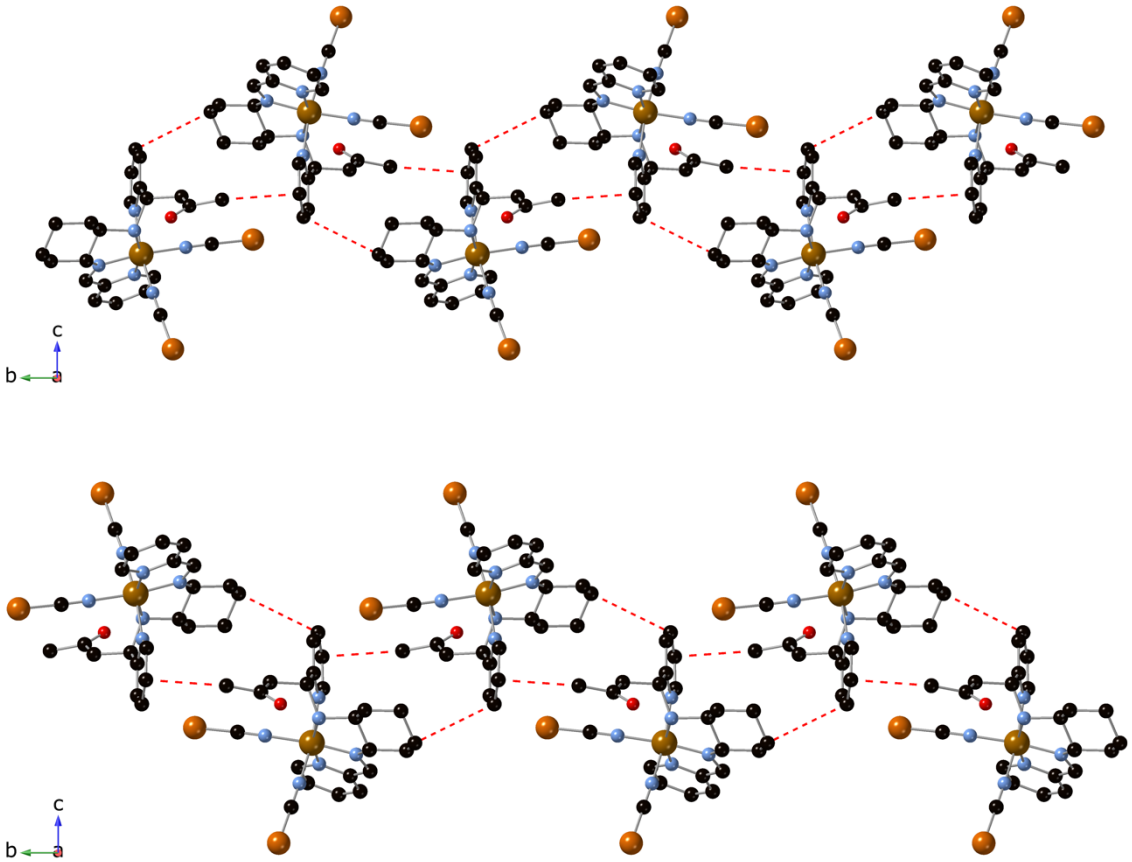

Fig. S6 Chains of complexes in the structure of [Fe(*RR*-*S*-L$_2$)(NCSe)$_2$] (top) and [Fe(*SS*-*R*-L$_2$)(NCSe)$_2$] (bottom) at 120 K linked through intermolecular interactions (red dashed lines).

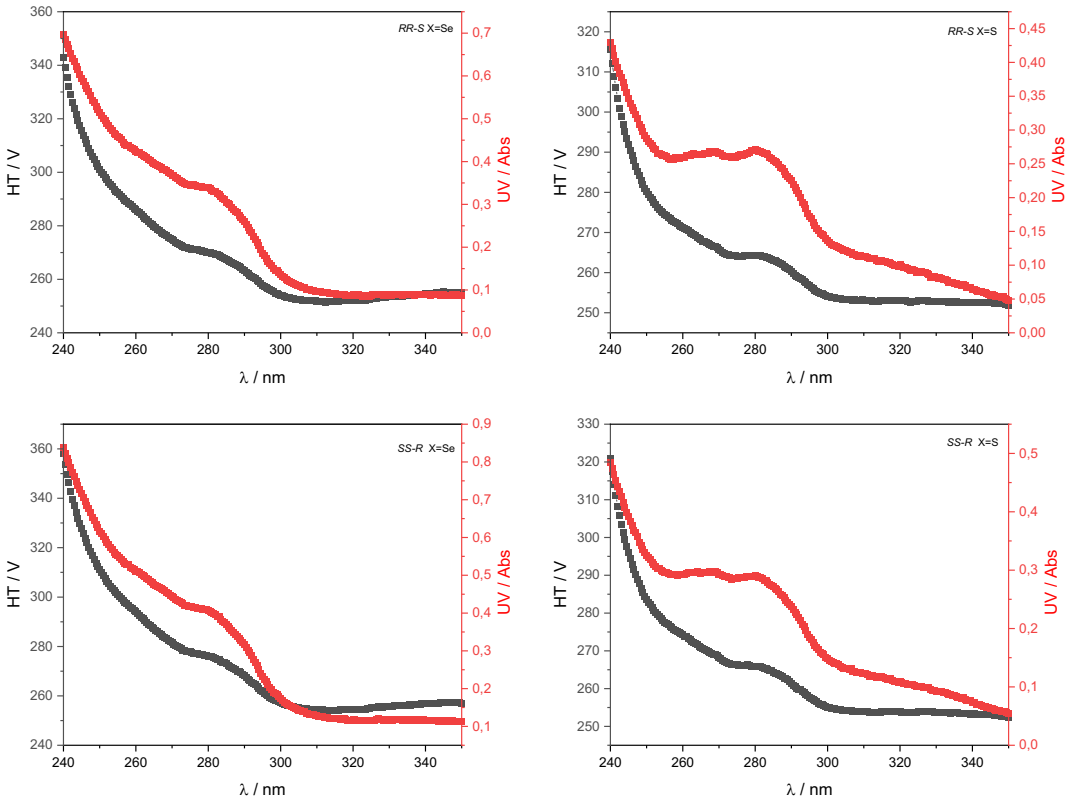

Fig. S7 UV-vis spectra and High Tension (HT) Voltage of CD measurements for 1 mM $CHCl_3$ solutions of [Fe(*RR*-*S*-L_2)$(NCSe)_2$] and [Fe(*SS*-*R*-L_2)$(NCSe)_2$] (left) and [Fe(*RR*-*S*-L_2)$(NCS)_2$] and [Fe(*SS*-*R*-L_2)$(NCS)_2$] (right).

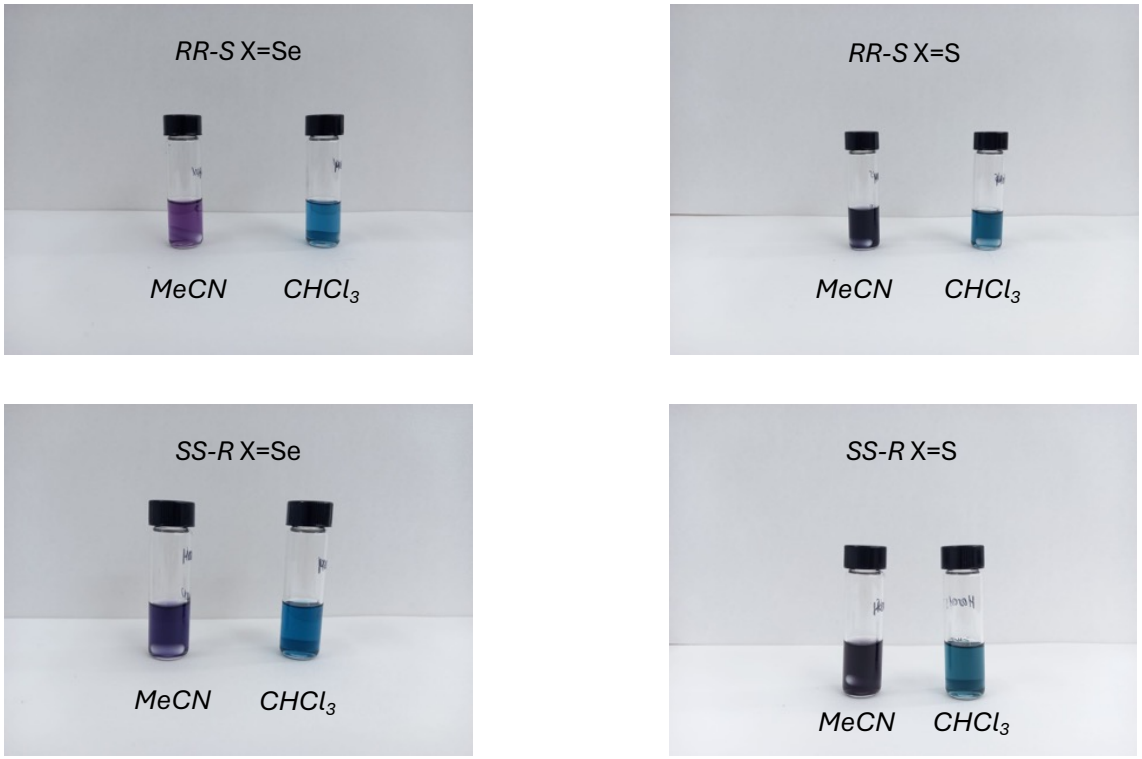

Fig. S8 Images of $CHCl_3$ and MeCN solutions of [Fe(*RR*-*S*- or *SS*-*R*-L_2)$(NCX)_2$].

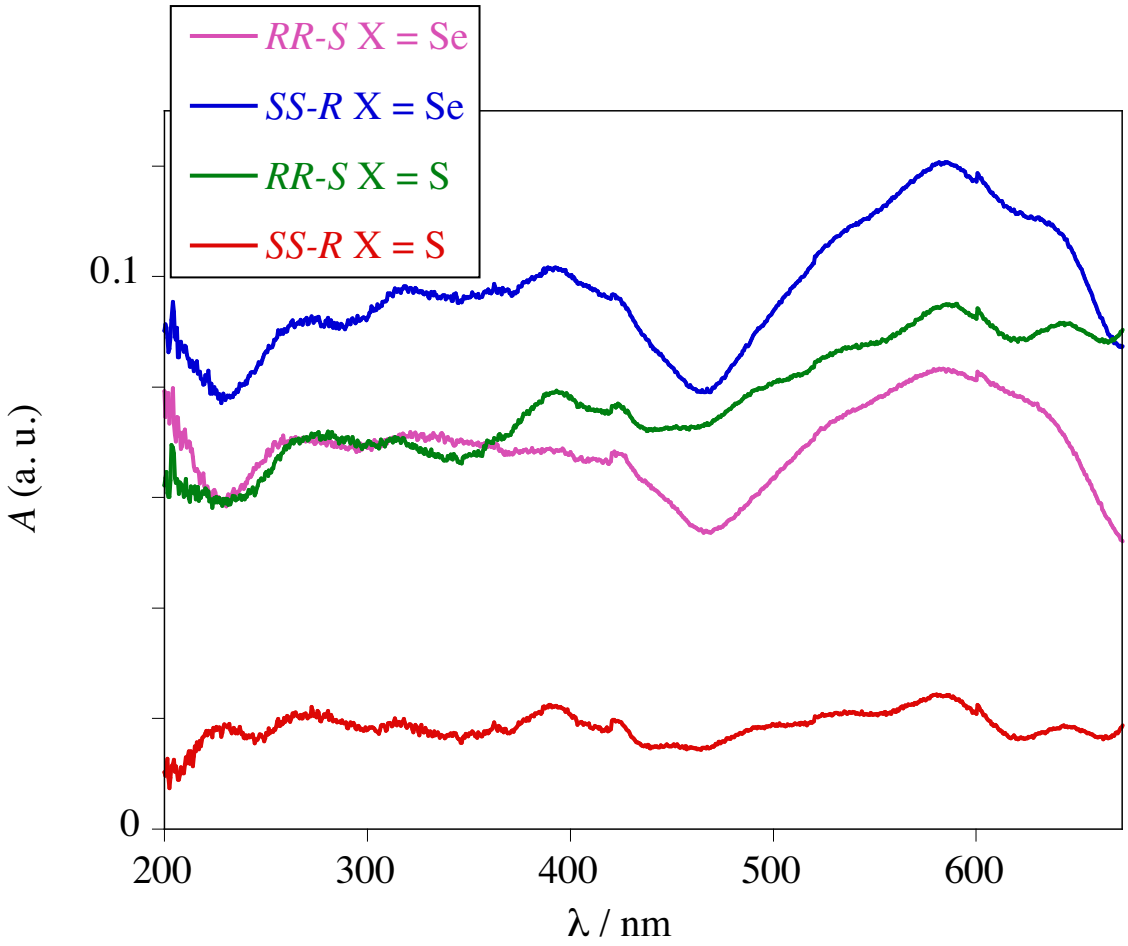

Fig. S9 Absorbance spectra of [Fe(*RR*-*S*- or *SS*-*R*-L_2)$(NCX)_2$] in the solid state.

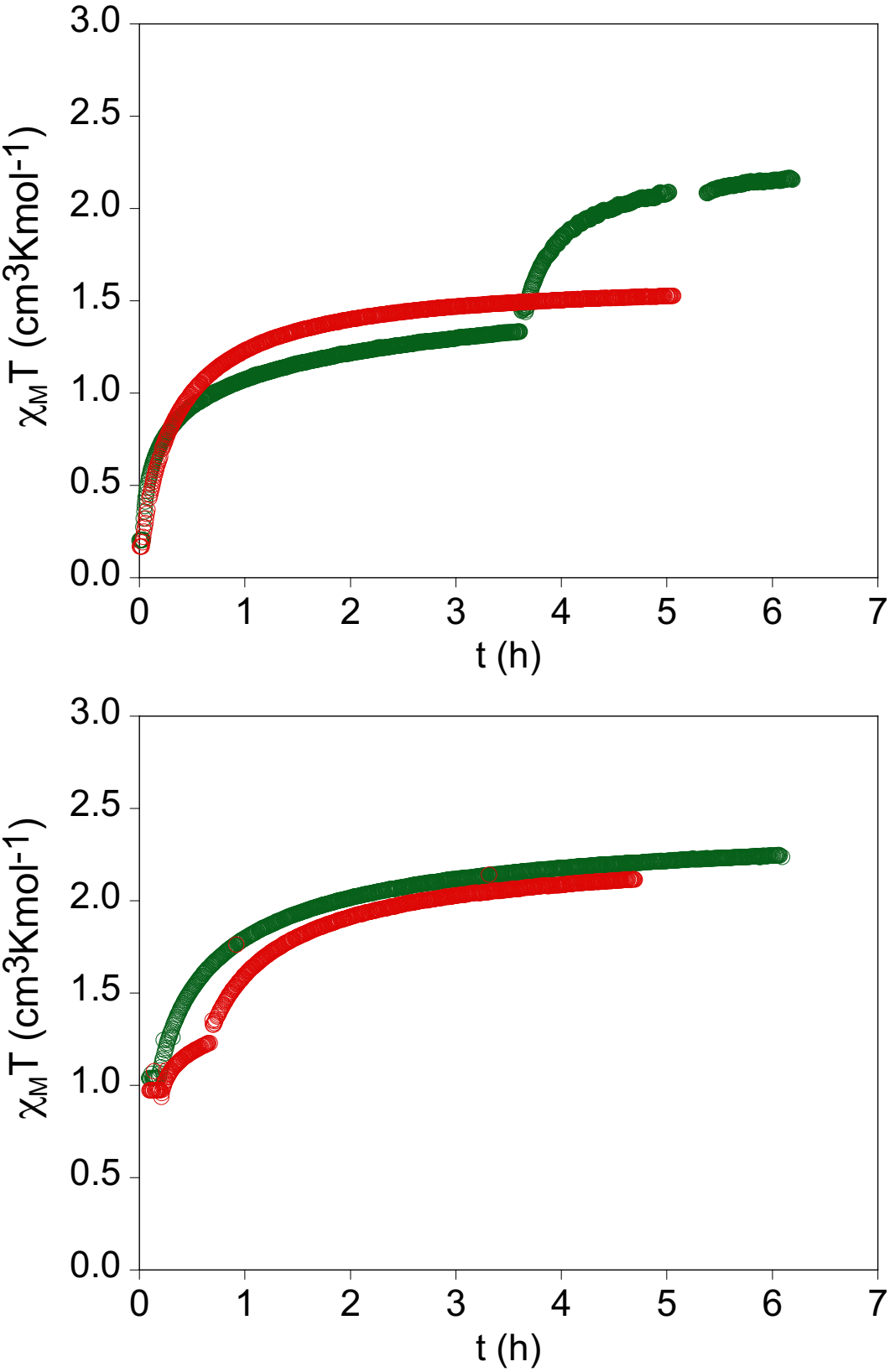

Fig. S10 Time variation of $\chi_M T$ for [Fe(*RR*-*S*-L_2)$(NCSe)_2$] (green circles) and [Fe(*SS*-*R*-L_2)$(NCSe)_2$] (red circles) (**top**), [Fe(*RR*-*S*-L_2)$(NCS)_2$] (green circles) and [Fe(*SS*-*R*-L_2)$(NCS)_2$] (red circles) (**bottom**) after irradiation at 10 K with 808 nm in the LIESST experiments from **Fig. 5**. [Fe(*RR*-*S*-L_2)$(NCSe)_2$] and [Fe(*SS*-*R*-L_2)$(NCS)_2$] were first irradiated with 660 nm (3.4 h for [Fe(*RR*-*S*-L_2)$(NCSe)_2$] and 0.5 h for [Fe(*SS*-*R*-L_2)$(NCS)_2$]).